Available online at www.sciencedirect.com
ScienceDirect
Nuclear Instruments and Methods in Physics Research B 00 (2017) 1–13
Nucl Instrum Meth B

Determination of the ^{64}Zn,^{47}Ti(n,p) Cross Sections using a DD Neutron Generator for Medical Isotope Studies

A.S. Voyles[a,*], M.S. Basunia[b], J.C. Batchelder[a], J.D. Bauer[c], T.A. Becker[d], L.A. Bernstein[a,b], E.F. Matthews[a], P.R. Renne[d,e], D. Rutte[d,e], M.A. Unzueta[a], K.A. van Bibber[a]

[a] *Department of Nuclear Engineering, University of California, Berkeley, Berkeley CA, 94720 USA*
[b] *Lawrence Berkeley National Laboratory, Berkeley CA, 94720 USA*
[c] *Lawrence Livermore National Laboratory, Livermore CA, 94551 USA*
[d] *Berkeley Geochronology Center, Berkeley CA, 94709 USA*
[e] *Department of Earth and Planetary Sciences, University of California, Berkeley, Berkeley CA, 94720 USA*

Abstract

Cross sections for the ^{47}Ti(n,p)^{47}Sc and ^{64}Zn(n,p)^{64}Cu reactions have been measured for quasi-monoenergetic DD neutrons produced by the UC Berkeley High Flux Neutron Generator. The study was motivated by interest in the production of ^{47}Sc and ^{64}Cu as emerging medical isotopes. The cross sections were measured in ratio to the ^{113}In(n,n')^{113m}In and ^{115}In(n,n')^{115m}In inelastic scattering reactions on co-irradiated indium samples. Post-irradiation counting using an HPGe and LEPS detectors allowed for cross section determination to within 5% uncertainty. The cross sections were determined with lower uncertainty than existing measurements and are found to be in good agreement with both empirical and theoretical values. This work highlights the utility of using DD plasma-based neutron sources for a host of nuclear data measurements and potentially for the production of radionuclides for medical applications.

ASV: Karl: "Comment to engender some discussion. I have a small concern here, reminiscent of what happened to our electron backstreaming paper in PRAB. To be publishable, even in NIMB, there has to be a crisp research question resolved, or some innovation. I think an angle that is missing here is that this is a new design of neutron generator, whose design maximizes the flux density (n/sec/cm2), although the total flux, while respectable, is not spectacular in itself. This is Lee's recent mantra, and I now understand its significance. Problematically, as Andrew has pointed out, we don't have the actual instrument paper published yet, so the thrust of the paper can't be too focused on the flux density issue, but a workable angle would be 'given we have this new capability, this is an example of its power'. Let me suggest Lee provide a sentence for the abstract, and a few sentences of text in the appropriate spot."

ASV: The abstract is now nicely short and sweet, but should it be expanded at all?

Todo list

1. Introduction

There has been significant interest in the past several years in exploring the use of neutron-induced reactions to create radionuclides for a wide range of applications. This interest is due to the volumetric absorption of neutrons as compared to charged particle beams (ranges of g/cm^2 as compared to 10's of mg/cm^2), together with the fact that isotope production facilities often produce large secondary neutron fields. Particular interest has been paid to (n,p) and (n,α) charge-exchange reactions since these reactions produce high-specific activity radionuclide samples without the use of chemical carriers in the separation process.

Two other potential neutron sources for (n,x) reactions exist in addition to the secondary neutron fields generated at existing isotope production facilities: reactors and neutron generators that utilize the D(T,n)α ("DT") and D(D,n)^{3}He ("DD") reactions. While reactors produce copious quantities of neutrons, their energy spectra is often not well-suited to the preparation of high-purity samples due to the co-production of unwanted activities via neutron capture, in addition to the significant start-up costs and proliferation concerns involved in their commissioning [1]. Similarly, while the higher energy 14-15 MeV neutrons produced at DT generators are capable of initiating (n,p) and (n,α) reactions, their higher energy opens the possibility of creating unwanted activities via (n,pxn) and (n,αxn) reactions that cannot easily be separated from the desired radionuclides.

In contrast, the neutron spectrum from a DD reaction, which ranges from approximately 2-3 MeV, is ideally suited to (n,p) radionuclide production. However, the lower achievable flux from these generators limits their production capabilities. An additional complication is the relative paucity of high-quality, consistent cross section data for neutrons in the 2-3 MeV DD energy range.

*Corresponding author
Email address: andrew.voyles@berkeley.edu (A.S. Voyles)

The purpose of the present work is to explore the potential to use high-flux neutron generators to produce high-specific activity samples of radionuclides at the mCi level for local use in the application community.

ASV: Karl: "A comment, hopefully not too gratuitous at this point, could be inserted here to the effect that if the promise of plasma-based DD generators is ultimately borne out, not only is it anticipated that most hospitals could have their own source affordably, but that it would open up a whole new realm of very short lifetime medical isotopes. Lee to be the arbiter of whether this is prudent or not."

The research group at UC Berkeley has developed a High Flux Neutron Generator (HFNG) that features an internal target where samples can be placed just several millimeters from the neutron producing surface in order to maximize the utilization of the neutron yield for the production of a desired radionuclide [2, 3]. The HFNG uses the D(D,n)^{3}He reaction to produce neutrons with energies near 2.45 MeV together with a self-loading target design to maintain continuous operation without target replacement. In addition to the generator itself, efforts are underway to design neutron reflection capabilities to allow scattered neutrons multiple opportunities to interact with an internally mounted target. While these design efforts are underway, the HFNG can be used to better characterize production cross sections at the appropriate neutron energy.

The present work features a pair of cross section measurements for the production of two non-standard positron emitters: ^{64}Zn(n,p)^{64}Cu and ^{47}Ti(n,p)^{47}Sc. ^{64}Cu ($t_{1/2}$ = 12.7 h) undergoes β^+ decay (61.5% branching ratio) to ^{64}Ni or β^- decay (38.5% branching ratio) to ^{64}Zn [4]. The emitted short-range 190-keV β^- particle makes this an attractive therapeutic radionuclide, which also has the possibility for simultaneous positron emission tomography (PET) imaging for real-time dose monitoring and verification. This makes ^{64}Cu particularly desirable for emerging radiation therapy protocols [5, 6, 7, 8]. In addition, copper radiochemistry is well developed, and many existing ligands and carriers may be used for selective delivery of the radionuclide to different sites in patients. The second radionuclide studied, ^{47}Sc ($t_{1/2}$ = 3.35 d), undergoes β^- decay to ^{47}Ti, emitting a high-intensity (63.8%) 159-keV gamma ray in the process [9]. This radionuclide is attractive as an emerging diagnostic isotope, due to the similarity of the emitted gamma ray to that of the well-established ^{99m}Tc [10, 11, 12, 13]. Due to the short half-life ($t_{1/2}$ = 6.0 h) of and dwindling supplies of ^{99m}Tc, ^{47}Sc stands poised as a potential solution to this shortage, due to its longer half-life and multiple production pathways without the need for highly enriched uranium [14]. In addition, when paired with ^{44}Sc, ^{47}Sc forms a promising "theranostic" pair for use in simultaneous therapeutic and diagnostic applications [15, 16].

Current methodology in radiochemistry has shown recovery of upwards of 95% of produced ^{64}Cu [17, 18] and ^{47}Sc [19, 20, 21] from solid target designs, without the need for additional carrier. By expanding the base of efficient reaction pathways, great advances can be made in making production of medical radionuclides more efficient and affordable for those in need.

2. Experiment

2.1. Neutron source

Neutron activation was carried out via irradiation in the High-Flux Neutron Generator (HFNG), a DD neutron generator at the University of California, Berkeley. This generator extracts deuterium ions from an RF-heated deuterium plasma through a nozzle, whose shape was designed to form a flat-profile beam, 5 mm in diameter. This deuterium beam is incident upon a water-cooled, self-loading titanium-coated copper target [2, 3], where the titanium layer acts as a reaction surface for DD fusion, producing neutrons with a well-known energy distribution as a function of emission angle [22]. Irradiation targets are inserted in the center of the titanium layer deuteron target, approximately 8 mm from the DD reaction surface, prior to startup. Figure 1 displays a cut-away schematic of the HFNG. A 100 kV deuterium beam was extracted at 1.3 mA, creating a flux of approximately $1.3 \cdot 10^7$ neutrons/cm^{2}s on the target.

2.2. Cross section determination by relative activation

The approach used in both measurements was to irradiate foils of zinc or titanium, which were co-loaded with indium foils in order to determine their (n,p) cross sections relative to the well-established ^{113}In(n,n')^{113m}In and ^{115}In(n,n')^{115m}In neutron dosimetry standards [23, 24]. Table 1 records physical characteristics of each foil for the various irradiations. In each experiment, the co-loaded foils were irradiated for 3 hours at nominal operating conditions of 1.3 mA and 100 kV. After irradiation, the foils

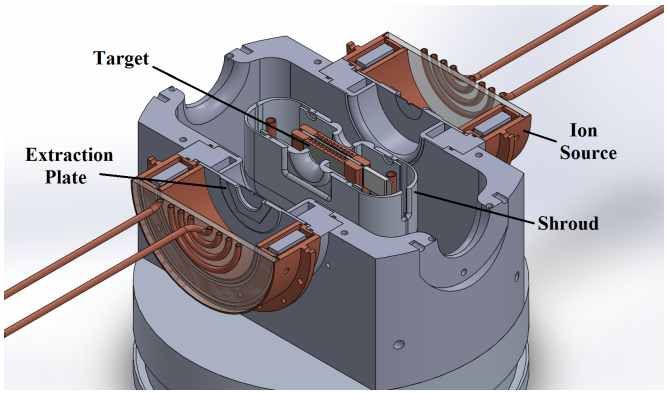

Figure 1. Cut-away schematic of the HFNG. The ion source is approximately 20 cm in diameter.

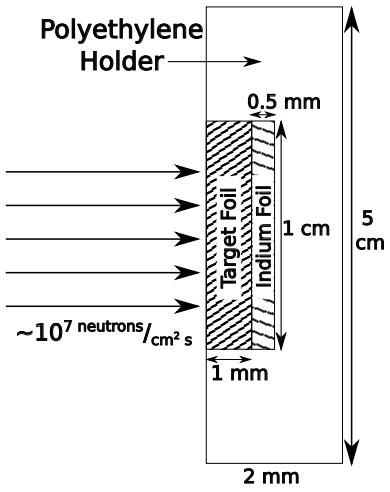

Figure 2. Schematic (not drawn to scale) of the sample holder used for the Berkeley HFNG,

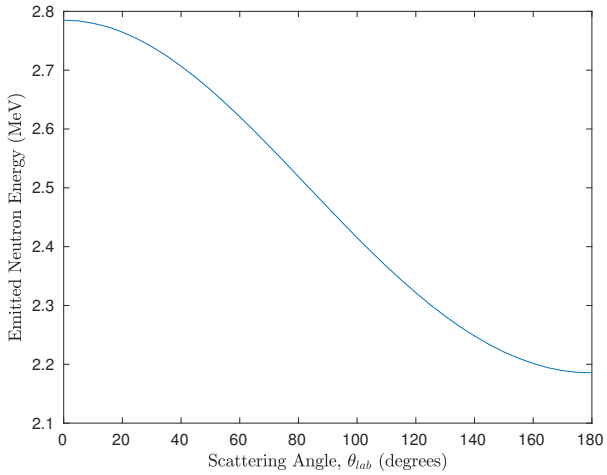

Figure 3. Energy-angle distribution for neutrons emitted following DD fusion, for 100 keV incident deuterons.

were removed and placed in front of an appropriate High-Purity Germanium (HPGe) gamma-ray detector and time-dependent decay gamma-ray spectra were collected.

One cm diameter, 1-mm thick natural abundance zinc and titanium targets were employed for the measurement. Each of these was co-loaded with a natural abundance Indium foil of 1 cm diameter and 0.5 mm thickness in a recess cut into a 2-mm thick polyethylene holder, as seen in Figure 2, which was mounted in the HFNG target center. Prior to loading, each foil was washed with isopropanol and dried, to remove any trace oils or residue that could become activated during irradiation.

2.3. Determination of effective neutron energy

The D(D,n)^{3}He reaction at 100 keV lab energy produces neutrons with energies ranging from 2.18 to 2.78 MeV, over an angular range of 0-180° in the lab frame-of-reference with respect to the incident deuteron beam. This distribution has been well documented [22] and is shown in Figure 3 for 100 keV incident deuteron energy.

Since the samples are separated by only 8 mm from the DD reaction surface they subtend a fairly significant (~17°) angular range in a region of impressive (approximately $1.3 \cdot 10^7$ neutrons/cm^{2}s) neutron flux. This stands in contrast to other measurements which feature collimated beams and significantly lower total neutron flux.

ASV: Does Figure 4 serve any purpose? I'm starting to think it doesn't - should we just cut it?

The Monte Carlo N-Particle transport code MCNP6 [25] was used to model the neutron energy spectrum incident upon target foils co-loaded into the HFNG (see Figure 5). This spectrum, peaked around 2.75 MeV, illustrates the forward-focused kinematics of the DD reaction subtended by the co-loaded sample foils.

While this shows that the sample foils experience a very narrow energy distribution of incident neutrons, an effective neutron energy window must be determined. The

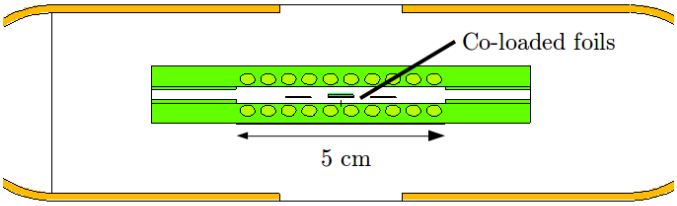

Figure 4. MCNP6 model of the HFNG target chamber, with reference scale. The co-loaded foils can be seen in the target chamber center. The ovals indicate the location of water cooling channels.

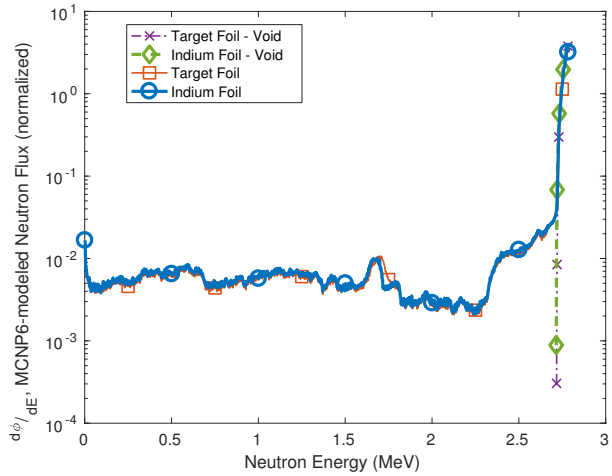

Figure 5. MCNP6-modeled neutron energy spectrum for the HFNG. The solid lines show the spectrum at the location of the indium and the target foil respectively. The dotted and dashed lines show the same with the target itself "voided" to remove scattering contributions. Less than 1% of the neutrons incident on the foils can be attributed to scatter in the neutron production target.

Table 1. Foil characteristics for each of the three (Zn/In)* experiments and the two (Ti/In)† experiments.

Foils Used	Metal Purity	Abundance (a/o)	Foil Density (mg/cm^2)	Thickness (mm)	Diameter (mm)	Mass (g)
^{nat}In	>99.999%	^{113}In (4.29%), ^{115}In (95.71%)	317.6	0.49 ± 0.02*	9.75 ± 0.09*	0.248 ± 0.005*
				0.50 ± 0.03*	9.98 ± 0.15*	0.248 ± 0.005*
				0.49 ± 0.03*	9.96 ± 0.10*	0.241 ± 0.005*
				0.53 ± 0.06†	10.01 ± 0.11†	0.247 ± 0.005†
				0.50 ± 0.02†	10.00 ± 0.09†	0.248 ± 0.005†
^{nat}Zn	>99.99%	^{64}Zn (49.17%)	698.9	1.03 ± 0.01	9.93 ± 0.14	0.538 ± 0.005
				1.03 ± 0.01	9.76 ± 0.17	0.521 ± 0.005
				1.02 ± 0.01	9.89 ± 0.15	0.542 ± 0.005
^{nat}Ti	99.999%	^{47}Ti (7.44%)	434.7	1.16 ± 0.02	9.93 ± 0.04	0.337 ± 0.005
				1.15 ± 0.02	9.94 ± 0.03	0.337 ± 0.005

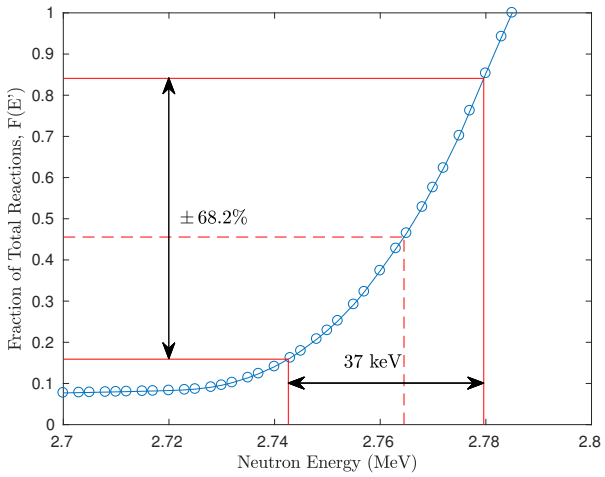

Figure 6. Fraction of total reactions induced in the Indium foil between the energies [0, E']. The red arrows indicate the energy region that corresponds to 67% of the total activation.

MCNP6 simulation shows an identical flux-weighted average neutron energy of 2.765 MeV for both the Indium and target foils to the 1 keV level. Due to the kinematics of DD neutron emission, E_{max}, the maximum energy of a neutron subtending the target foils in this geometry is 2.783 MeV [22]. For this maximum energy, the number of reactions induced in a foil (containing N_i target nuclei) is given by:

$$R = N_i \int_0^{E_{max}} \sigma(E) \frac{d\phi}{dE} dE \tag{1}$$

From this definition, it is possible to calculate $F(E')$, the fraction of total reactions induced by neutrons up to some energy $E' < E_{max}$:

$$F(E') = \frac{\int_0^{E'} \sigma(E) \frac{d\phi}{dE} dE}{\int_0^{E_{max}} \sigma(E) \frac{d\phi}{dE} dE} \tag{2}$$

This quantity $F(E')$ is plotted in Figure 6. The fraction of total reactions in the indium foil can be used to characterize the effective neutron energy bin. Our approach, in analogy to the Gaussian quantity σ, will be to use a horizontal "error bar" to represent the energy range responsible for 68.2% of the reactions taking place. Using this approach, we report the effective energy bin as being E_n=2.765$^{+0.015}_{-0.022}$ MeV. This 37-keV full-energy spread verifies that, at such close distances to the DD reaction surface, loaded target foils receive a quasi-monoenergetic neutron flux.

2.4. Measurement of induced activities

After irradiation, the co-loaded targets were removed from the HFNG and transferred to a counting lab, where their induced activities could be measured via gamma ray spectroscopy. Two detectors were used in this measurement. An Ortec 80% High-Purity Germanium (HPGe) detector was used for the detection of the positron annihilation radiation from the ^{64}Cu decay [4], the 391 keV gamma-ray from the ^{113m}In isomer [26], and the 336 keV gamma-ray from the decay of the ^{115m}In isomer [27]. An Ortec planar Low-Energy Photon Spectrometer (LEPS) was used for the detection of the lower-energy 159 keV gamma-ray from ^{47}Sc [9] as well as the two indium isomers mentioned above. Both detectors were calibrated for energy and efficiency, using ^{133}Ba, ^{137}Cs, and ^{152}Eu sources at various distances from the front face of each detector. These efficiencies, along with gamma ray intensities for each transition, were used to convert the integrated counts in each gamma ray photopeak into an activity for the activated isotopes and isomeric states.

The irradiated foils were counted in their polyethylene holder, 10 cm from the front face of the 80% HPGe and 1 cm from the front face of the LEPS, with the target foil (zinc or titanium) facing towards the front face of the detector when both target and monitor foils were counted simultaneously. All data collection was performed using the Ortec MAESTRO software. For each experiment the detector dead time was verified to be less than 5%. No summing corrections needed to be made since all of the

Table 2. Gamma-ray properties for the decay lines measured in the present work.

Nuclide	Gamma-Ray Energy (keV)	Intensity (%)	$t_{1/2}$
^{64}Cu [4]	511.0	35.2 ± 0.4	12.701 h
^{47}Sc [9]	159.381	68.3 ± 0.4	3.3492 d
^{113m}In [26]	391.698	64.94 ± 0.17	99.476 m
^{115m}In [27]	336.241	45.9 ± 0.1	4.486 h
^{116m}In [28]	416.90	27.2 ± 0.4	54.29 m

gammas are either non-coincident or formed in a back-to-back annihilation event.

For the ^{47}Sc production experiments, the foils were counted simultaneously using a planar LEPS detector. For the ^{64}Cu production experiments, the Indium foil was first counted separately using an 80% HPGe detector, to capture the short-lived Indium activities. This is due to the fact that the contaminant ^{115}In(n,γ) reaction results in the production of ^{116m}In which has a 54 minute half-life and results in the production of 1097 keV (58.5% branching), 1293 keV (84.8% branching) and 2112 keV (15.09% branching) gamma-rays that in turn produce a significant number of 511 keV gammas from pair-production followed by annihilation [28]. The foils were counted together again after approximately 4 hours of separate collection, to allow for nearly all of the produced ^{116}In to decay. Example spectra for each production pathway can be seen in Figure 7a and Figure 7b.

To verify that each peak corresponds to the assigned decay product, spectra were acquired in a sequence of 15 - 30 minute intervals. The resulting time series displayed in Figures 8a - 8d allow the fitting of exponential decay functions for each nuclide and comparison of the measured half-life with literature values. The fitted functions for each transition agree (at the 1σ confidence level) with accepted half-lives [9, 4, 26, 27, 28], confirming the respective peak assignments.

The spectra for the different samples were summed and the net peak areas were fitted using gf3, part of the RadWare analysis package from Oak Ridge National Laboratory [29, 30]. The background-subtracted integrated counts in each photopeak, as well as the counting duration for each experiment, are tabulated in Table 3.

2.5. Experimental verification of incident neutron energy

As shown in subsection 2.2 above, the effective neutron energy depends on the angle range subtended by the sample with respect to the incident deuteron beam. In order to determine this angle it is necessary to measure the lateral location of the beam with respect to the sample location. This centroid position of the beam was measured using a 3 x 3 array of 0.5 cm diameter indium foils. The relative activity of these foils was then determined via post-irradiation counting of the ^{115m}In isomer ($t_{1/2}$ = 4.486 h) [27]. Figure 9 shows the measured activities for these 9

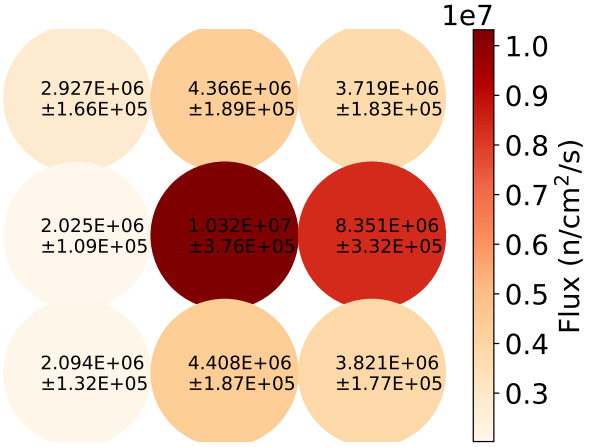

Figure 9. Relative fluxes as seen by a 3 x 3 array of indium foils. The central foil corresponds to the location in which target and monitor foils were mounted during the cross section measurements, verifying that the beam is centered on the middle of mounted foils.

indium foils. Based on these values we are able to verify that the beam was indeed centered on the middle of the zinc and titanium samples.

2.6. Calculation of measured cross sections

For a thin target consisting of N_T target nuclei (with a reaction cross section $\sigma\left(\bar{E}\right)$), subjected to a constant neutron flux $\phi\left(\bar{E}\right)$, the rate of production (R) of the product nucleus will be:

$$R = N_T \sigma\left(\bar{E}\right) \phi\left(\bar{E}\right) \tag{3}$$

If this irradiation lasts for some time t_1, and gamma ray spectrum acquisition begins at a later time t_2 and ends at t_3, then the number of product decays (D; with decay constant λ) during the acquisition will be:

$$\begin{aligned} D &= \frac{R}{\lambda}\left(e^{\lambda t_1} - 1\right)\left(e^{-\lambda t_3} - e^{-\lambda t_2}\right) \\ &= \frac{N_T \sigma\left(\bar{E}\right) \phi\left(\bar{E}\right)}{\lambda}\left(e^{\lambda t_1} - 1\right)\left(e^{-\lambda t_3} - e^{-\lambda t_2}\right) \end{aligned} \tag{4}$$

If this decay emits a gamma ray with absolute intensity I_γ (photons emitted per decay), and is detected with an absolute efficiency of ϵ_γ (photons detected / photons emitted), then the number of observed decays between t_2 and t_3 will be:

$$\begin{aligned} N_{obs} &= D \epsilon_\gamma I_\gamma \\ &= \epsilon_\gamma I_\gamma \frac{N_T \sigma\left(\bar{E}\right) \phi\left(\bar{E}\right)}{\lambda}\left(e^{\lambda t_1} - 1\right)\left(e^{-\lambda t_3} - e^{-\lambda t_2}\right) \end{aligned} \tag{5}$$

Solving this equation for the cross section results in:

$$\sigma\left(\bar{E}\right) = \frac{N_{obs}\lambda}{N_T \epsilon_\gamma I_\gamma \phi\left(\bar{E}\right)\left(e^{\lambda t_1} - 1\right)\left(e^{-\lambda t_3} - e^{-\lambda t_2}\right)} \tag{6}$$

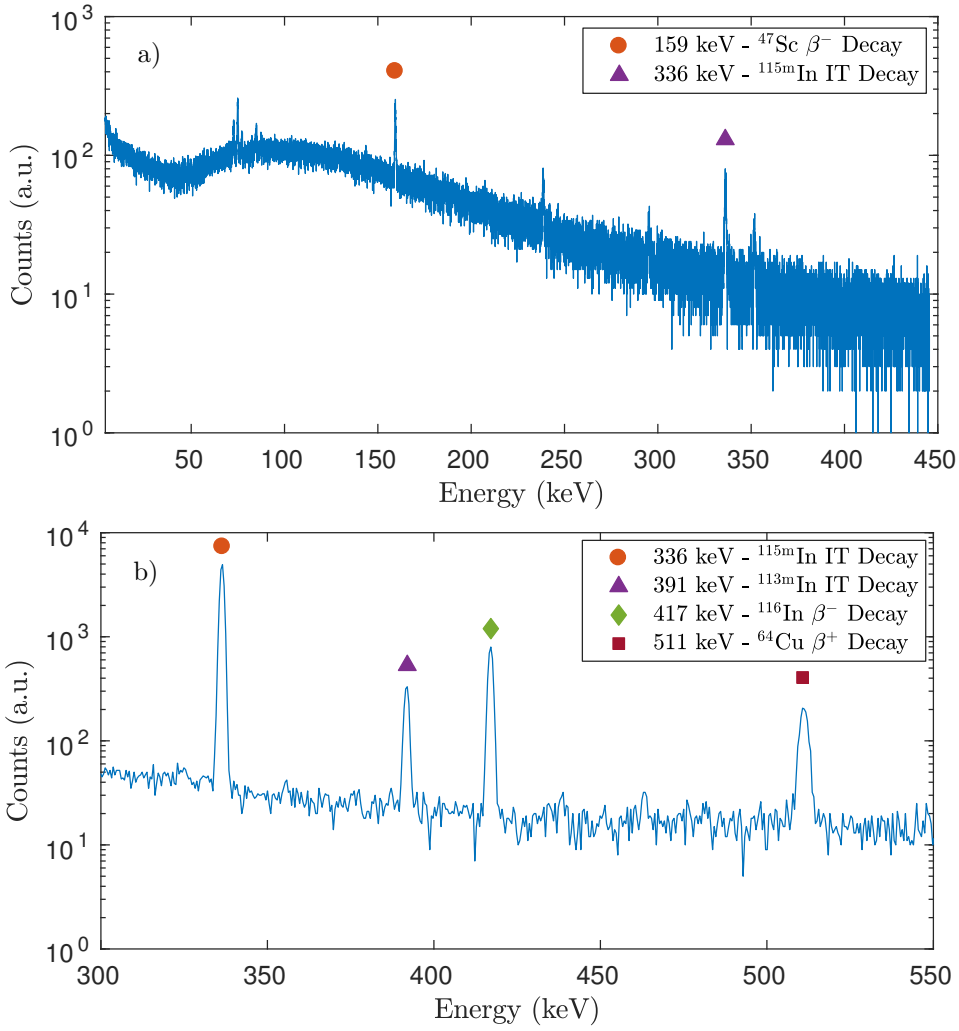

Figure 7. Example gamma spectra collected to monitor radioisotope production. (a) Gamma spectrum for the ^{47}Ti(n,p)^{47}Sc production pathway foils, counted using a LEPS detector and (b) gamma spectrum for the ^{64}Zn(n,p)^{64}Cu production pathway foils, counted using an 80% HPGe detector.

Equation 6 can be used to determine the unknown (n,p) cross sections relative to the well-known ^{115}In(n,n')^{115m}In and ^{113}In(n,n')^{113m}In inelastic scattering cross sections since the Zn and Ti samples were co-irradiated with indium foils. This approach has a number of advantages since the result is independent of neutron flux and only depends on the relative detector efficiencies at each gamma-ray energy. Equation 7 shows the ratio of the cross sections determined using this approach, in which subscript P indicates a quantity for either ^{64}Cu or ^{47}Sc, and subscript In indicates a quantity for either the ^{113m}In or ^{115m}In isomer. A minor term was added to correct for the small self-attenuation of the gamma rays emitted by the activated foils:

$$\frac{\sigma_P}{\sigma_{In}} = \frac{A_P}{A_{In}} \frac{N_{T,In}}{N_{T,P}} \frac{\lambda_P}{\lambda_{In}} \frac{e^{\lambda_{In} t_1} - 1}{e^{\lambda_P t_1} - 1} \times \times \frac{e^{-\lambda_{In} t_3} - e^{-\lambda_{In} t_2}}{e^{-\lambda_P t_3} - e^{-\lambda_P t_2}} \frac{\epsilon_{In}}{\epsilon_P} \frac{I_{\gamma,In}}{I_{\gamma,P}} \frac{e^{-\mu_{In} x_{In}/2} \times e^{-\mu_{In} x_P}}{e^{-\mu_P x_P/2}} \quad (7)$$

where:

- A is the integrated counts under a photopeak [counts],
- σ is the cross section for either the production of a product or isomer [mb],
- N_T is the initial number of target nuclei,
- λ is the decay constant [s^{-1}],
- t_1 is the irradiation time [s],
- t_2 is the time between the start-of-beam and the start of counting [s],
- t_3 is the time between the start-of-beam and the end of counting [s],
- ϵ is the detector efficiency for a particular photopeak,
- I_γ is the decay gamma ray absolute intensity [%],

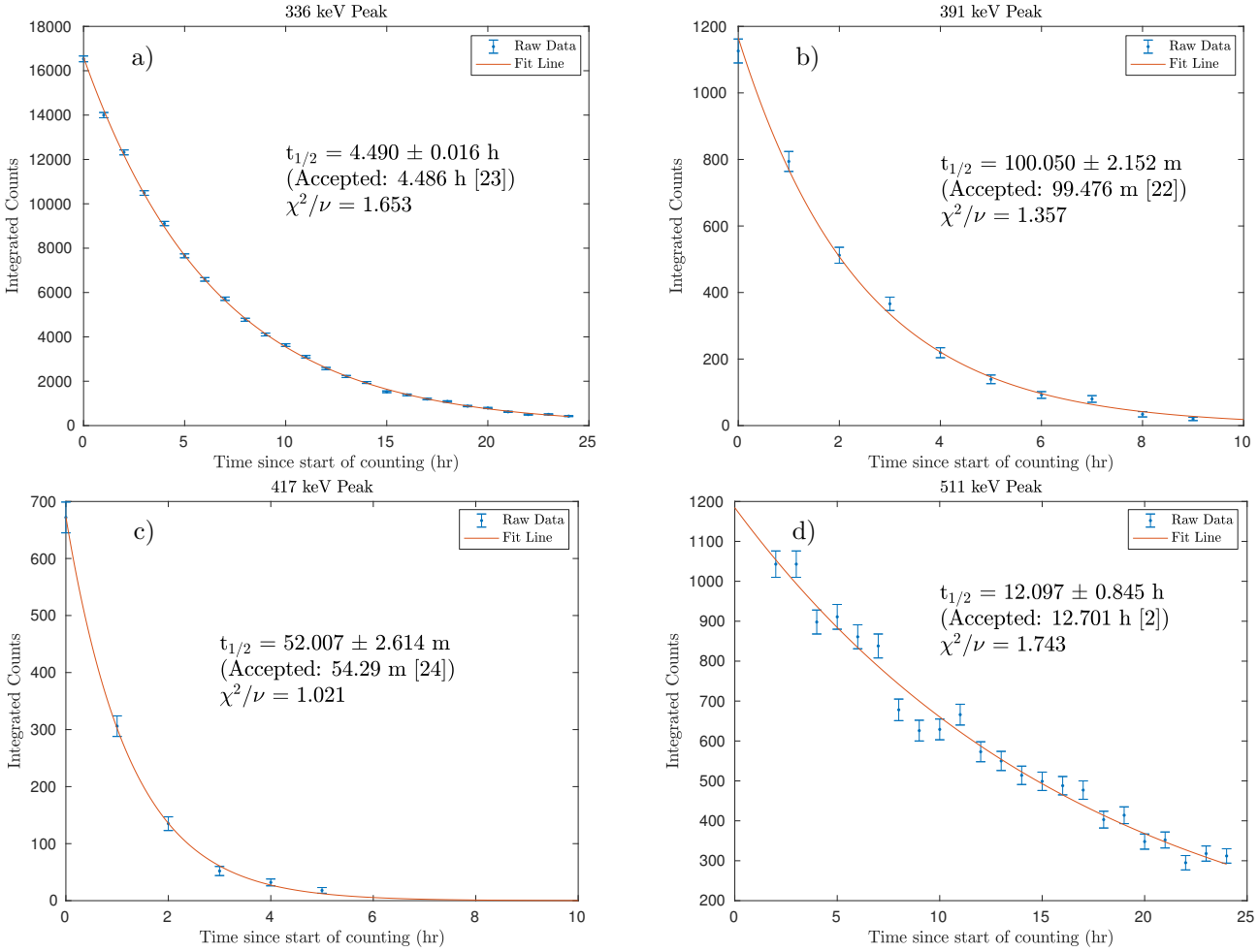

Figure 8. Decay curves used to verify photopeak transition assignment. (a) Decay curve for the isomeric transition of ^{115m}In, (b) decay curve for the isomeric transition of ^{113m}In, (c) decay curve for the β^- decay of ^{116}In, and (d) decay curve for the β^+ decay of ^{64}Cu.

Table 3. Counting times and photopeak counts for each of the (Zn/In) and (Ti/In) experiments. The uncertainties in photopeak counts are a combination of the fit error and counting statistics.

Reference Foil	^{nat}In	^{nat}In	^{nat}In	^{nat}In	^{nat}In
Reference Foil Mass (g)	0.248	0.248	0.241	0.247	0.248
Target Foil	^{nat}Zn	^{nat}Zn	^{nat}Zn	^{nat}Ti	^{nat}Ti
Target Foil Mass (g)	0.538	0.451	0.452	0.337	0.337
Irradiation Time, t_1 (s)	10800	10800	12629	11837	14254
Start of Count, t_2 (s)	12585	26985	14919	101245	16644
End of Count, t_3 (s)	103773	80993	68919	187669	110275
Photopeak Counts, 336 keV (^{115m}In)	113665 ± 1490	74321 ± 275	39895 ± 201	2122 ± 55	55102 ± 268
Photopeak Counts, 391 keV (^{113m}In)	3382 ± 171	860 ± 40	2545 ± 54	_____	_____
Photopeak Counts, 511 keV (^{64}Cu)	16055 ± 643	12852 ± 118	24464 ± 159	_____	_____
Photopeak Counts, 159 keV (^{47}Sc)	_____	_____	_____	3877 ± 83	5544 ± 257

- μ is the photon attenuation coefficient for a particular decay gamma ray in a foil [cm^{-1}],
- and x is the thickness of foil traversed by a particular decay gamma ray [cm]

In addition to the ^{115}In(n,n')^{115m}In reference cross section, the ^{115}In(n,γ)^{116m}In ($t_{1/2}$ = 54.29 min [28]) activity can be used to determine the ^{64}Zn(n,p) and ^{47}Ti(n,p) cross section. The capture activity is potentially subject to contamination from lower energy, especially thermal, "room return" neutrons since the (n,γ) cross section at 25 meV is approximately 2,000 times greater than at 2.7 MeV [23, 24].

With the exception of decay constants, which have negligible uncertainty compared to other sources of uncertainties in this work, each of the parameters in this model carries am uncertainty. Based on the assumption that these uncertainties are uncorrelated, the total relative statistical uncertainty δ_σ is calculated by taking the quadrature sum of the relative uncertainties of each parameter δ_i:

$$\delta_\sigma = \|\vec{\delta}\|_2 = \sqrt{\sum_{i=1}^{N} \delta_i^2} \tag{8}$$

This total uncertainty will be plotted as the cross section error bar in the excitation function for these production reactions.

2.7. Systematic uncertainties

The largest source of systematic uncertainty in the cross section determined via the "ratio approach" is the 2.586% uncertainty in the ^{115}In(n,n')^{115m}In cross section and the 1.447% uncertainty in the ^{113}In(n,n')^{113m}In cross section [23, 24]. An additional uncertainty arises from the fact that the Zn/Ti samples are not located at exactly the same location as the indium monitor foils, and are therefore not subject to precisely the same neutron flux. However, the MCNP6 simulations shown in Figure 5 indicate that the difference in the flux that the two foils are subjected to is less than 1%, negligible compared to other sources of systematic uncertainty. Other monitor foils could be used instead of indium, with ^{58}Ni(n,p)^{58}Co (^{58}Co $t_{1/2}$ = 70.86 d [31]) being one possible candidate, but the 4.486 hour and 99.476 minute half-lives of the ^{115m}In and ^{113m}In isomers [27, 26], respectively, makes indium a better candidate for measuring the production of radionuclides with lifetimes much less than 71 days. The largest source of uncertainty in energy window arises from uncertainties in the actual dimension of the deuteron beam on the production target. We believe, based on "burn marks" on the production target, that the beam was approximately circular, with a flat intensity profile and a 5 mm diameter. However, every 1 mm change in the beam radius would cause a 0.028 MeV shift in the centroid and a 0.053 MeV increase in the effective energy bin width.

Table 4. Results of cross section measurement. Note that the last data point for the ^{47}Sc measurement (marked with *) was performed at a slightly different beam spot location, leading to a difference in effective neutron energy.

Reaction	$\sigma(E_n$ = 2.7645 MeV) (mb)
^{64}Zn(n,p)^{64}Cu (relative to ^{113}In)	45.958 ± 2.553, 46.498 ± 1.745, 46.841 ± 3.170
^{64}Zn(n,p)^{64}Cu (relative to ^{115}In)	49.926 ± 3.190, 49.219 ± 2.709, 49.011 ± 2.540
^{47}Ti(n,p)^{47}Sc (relative to ^{115}In)	25.904 ± 1.193, 26.751 ± 1.394*

3. Results

Using the ratio method described, the cross sections for the ^{47}Ti(n,p)^{47}Sc and ^{64}Zn(n,p)^{64}Cu reactions have been calculated for incident neutron energy of $E_n = 2.765^{+0.015}_{-0.022}$ MeV. These values are recorded in Table 4.

ASV: Karl: "For the figures, let me suggest you make a red solid rectangle whose dimensions represent the error bars in both energy and cross section. Then put a large red circle around it, whose diameter is of order 10% of the size of the whole graph, to focus the eyes. In the caption, mention that the size of the rectangle represents the error limits."

Figures 10 and 11 present the determined cross sections for the production of ^{47}Ti(n,p)^{47}Sc and ^{64}Zn(n,p)^{64}Cu relative to literature data retrieved from EXFOR [32, 33, 34, 35, 36, 37, 38, 39, 40, 41, 42, 43, 44, 45, 46]. The weighted average of the measurements give 46.415 ± 1.720 mb (relative to ^{113}In) and 49.315 ± 2.567 mb (relative to ^{115}In) for ^{64}Zn(n,p)^{64}Cu, and 26.262 ± 0.822 mb for ^{47}Ti(n,p)^{47}Sc. The ^{64}Zn(n,p)^{64}Cu cross section measured in this work is consistent with other literature results, but with a smaller uncertainty (<5%). However, in the case of the ^{47}Ti(n,p)^{47}Sc cross section, our results are consistent with the results from the Smith (1975), Armitage (1967), and Ikeda (1990) groups [37, 43, 44] and both the ENDF/B-VII.1 [47] and TALYS [48] values, but significantly below the results from Hussain (1983), Gonzalez (1962), and Shimizu (2004) [39, 42, 46].

As mentioned above, the cross section can be obtained relative to both the inelastic scattering cross sections on ^{113}In and ^{115}In, and the capture of fast, unmoderated neutrons on ^{115}In. The results from both are consistent, indicating that the contributions from thermal "room return" neutrons are negligible for samples mounted in the center of the HFNG. This builds confidence in our results, and highlights the potential of using the HFNG for fast neutron capture reactions via activation. This will be discussed in greater detail in the conclusion section below.

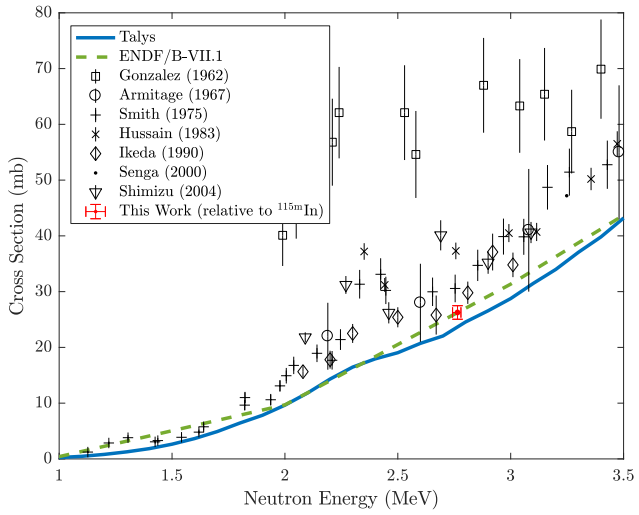

Figure 10. Measured ^{47}Ti(n,p)^{47}Sc cross section relative to indium activation.

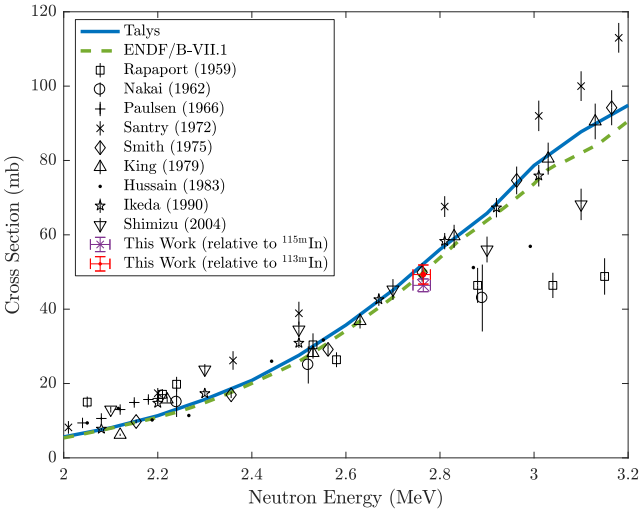

Figure 11. Measured ^{64}Zn(n,p)^{64}Cu cross section relative to indium activation.

ASV: The capture cross sections are actually consistent with effective 2.45 MeV neutrons (which are still fast). For capture of 2.76 MeV neutrons, we predict (n,p) cross sections approx. 15 mb less than using the In(n,n') monitors. How can we incorporate best this? Please suggest language changes / additions. Since they are only consistent at 2.45 MeV, I removed the points from Figures 10 and 11, but will happily add them back if someone thinks they serve a purpose.

ASV: Batch - in both figs 10 and 11, our value is hard to see, esp. in black and white... How to improve this, since there are so many experimental sets? Bigger symbols (this makes the centroid harder to see)? arrow pointing to it? Circle it?

4. Conclusion

Using activation methods on thin foils, the ^{47}Ti(n,p)^{47}Sc and ^{64}Zn(n,p)^{64}Cu production cross sections were measured for $2.765^{+0.015}_{-0.022}$ MeV neutrons produced using the High Flux Neutron Generator (HFNG) at UC Berkeley. The cross sections were measured with less than 5% uncertainty relative to the well-known ^{115}In(n,n')^{115m}In and ^{113}In(n,n')^{113m}In fast neutron cross sections [23, 24]. The measured values of 26.262 ± 0.822 mb and 46.415 ± 1.720 mb (relative to ^{113}In) or 49.315 ± 2.567 mb (relative to ^{115}In), respectively, are consistent with earlier experimental data and theoretical models, but have smaller uncertainties than previous measurements. In addition, the results for the production of ^{116}In via the ^{115}In(n,γ) reaction was shown to be consistent with activation from the capture of fast (e.g., ≈2.45 MeV) neutrons, rather than from "room return" thermal neutrons.

ASV: Karl: "You may wish to add a statement that this is a significant finding of this work. It wasn't a foregone conclusion that it would work out this way, given the several order of magnitude difference in cross section."

The use of DD neutron generators can be an efficient method for the measurement of low-energy (n,p) reaction channels, as well as a relative method used to normalize measurements at higher neutron energies.

ASV: Use correct fast neutron energy above

The proximity of the target to the neutron production surface also opens the possibility of performing a measurement of the cross section over a limited energy range via mounting the samples slightly off-axis with respect to the beam. This could be accomplished using the 9-foil sample holder described in subsection 2.5 above. Mounting samples at each of these positions would subject the samples to neutrons with energies ranging from 2.765 MeV at the central location to 2.616 MeV at the four corners, with the other locations having intermediate energy values. These sorts of multi-sample measurements could be used to de-

termine the "rising edge" of the cross sections, aiding in the development of optical models for the reactants.

These measurements also highlight the possibility of using fast neutrons from DD and/or DT generators to produce meaningful quantities of radioisotopes for a wide range of applications via charge exchange reactions, such as (n,p) and (n,α). Many applications, including diagnostic and therapeutic medical use, require mCi activity levels. The production of a radionuclide sample with an activity A driven to secular equilibrium using a neutron source with a total flux ϕ and a reaction cross section σ acting on sample of N_{target} atoms is given by the expression:

$$A = \lambda N_{product} = \eta \phi \sigma N_{target} \tag{9}$$

where we have introduced the dimensionless *neutron utilization factor* η, which represents the likelihood of a neutron inducing the desired reaction on one of the target sample atoms:

$$\eta = \int_0^E \mathrm{d}E_n \frac{\sigma_{(n,p)}}{\sigma_{(n,x)} + \sigma_{(n,p)}} \int N_{target}\,(r,\theta,\varphi)\,\mathrm{d}\mathbf{V},$$
$$\mathrm{d}\mathbf{V} = r^2 \mathrm{d}r \sin\theta\,\mathrm{d}\theta\,\mathrm{d}\varphi \tag{10}$$

An optimal design for the neutron generator would also allow for the possibility of reflecting fast neutrons back onto the target to maximize their utilization for radionuclide production. This sort of "flux trap" has been used for the production of radionuclides in reactors, but has not to date been optimized for use with fast neutrons at DD and/or DT neutron sources. The HFNG, with its self-loading target and "flux trap" geometry, has many features that make it well-suited for such isotope production purpose. Switching to DT operation would dramatically increase the flux as well as the production cross section, since (n,p) tends to be significantly larger at 14 MeV. However, the higher neutron energy would also open the (n,pn) channels. In the case of ^{47}Sc, this would lead to the presence of ^{46}Sc ($t_{1/2}$ = 83.79 d [49]) in the sample, which might pose some concerns for medical applications. However, this is not an issue for ^{64}Cu since the (n,pn) channel leads to the production of stable ^{63}Cu.

ASV: Karl: "Excellent paragraph. You may with to say that the HFNG is now operating at 10^9 n/sec, with a clear path towards 10^{10}, and a design study is underway for such a neutron-reflector assisted HFNG for actual medical isotope production."

In closing, we have measured the ^{64}Cu(n,p) and ^{47}Ti(n,p) cross sections for 2.765 MeV incident neutrons. In addition to improving the value of these measurements nuclear reaction evaluation, our results highlight the potential use of compact neutron generators for the production of radionuclides locally for medical applications. In the future we plan to perform additional cross section measurements at the HFNG, and to explore methods to extract the radionuclides from the sample using both chemical and physical separation techniques.

Future work will involve the continued measurement of the (n,p) production cross sections for various other emerging therapeutic and diagnostic radioisotopes, to expand the toolset of options available for modern medical imaging and cancer therapy. This will focus on radionuclides which permit more customized and precise dose deposition, as well as patient-specific treatments.

5. Acknowledgements

This work has been carried out at the University of California, Berkeley, and performed under the auspices of the U.S. Department of Energy by Lawrence Livermore National Laboratory under contract # DE-AC52-07NA27344 and Lawrence Berkeley National Laboratory under contract # DE-AC02-05CH11231. Funding has been provided from the US Nuclear Regulatory Commission, the US Nuclear Data Program, NSF ARRA Grant # XXXXXXXX, the University of California Laboratory Fees Research Grant # 12-LR-238745, and DFG Research Fellowship # RU 2065/1-1.

ASV: Add NSF Grant number from P. Renne.

We acknowledge Glenn Jones of G&J Jones Enterprises of Dublin, CA for the construction and commissioning of the High Flux Neutron Generator.

References

[1] D. Updegraff, S. A. Hoedl, Nuclear Medicine without Nuclear Reactors or Uranium Enrichment.

[2] C. Waltz, M. Ayllon, T. Becker, L. Bernstein, K.-N. Leung, L. Kirsch, P. Renne, K. V. Bibber, Beam-induced Back-streaming Electron Suppression Analysis for an Accelerator Type Neutron Generator Designed for 40Ar/39Ar Geochronology, Applied Radiation and Isotopes 125. arXiv:1701.00300, doi:10.1016/j.apradiso.2017.04.017.

[3] C. Waltz, Characterization of Deuteron-Deuteron Neutron Generators, Ph.D. thesis, University of California, Berkeley (2016).

[4] B. Singh, Nuclear Data Sheets for A = 64, Nuclear Data Sheets 108 (2) (2007) 197–364. doi:10.1016/j.nds.2007.01.003.

[5] M. R. Lewis, M. Wang, D. B. Axworthy, L. J. Theodore, R. W. Mallet, A. R. Fritzberg, M. J. Welch, C. J. Anderson, In Vivo Evaluation of Pretargeted 64Cu for Tumor Imaging and Therapy, Journal of Nuclear Medicine 44 (8) (2003) 1284–1292.

[6] NSAC Isotopes Subcommittee, Meeting Isotope Needs and Capturing Opportunities for the Future: The 2015 Long Range Plan for the DOE-NP Isotope Program, Tech. rep. (jul 2015).

[7] R. P. Bandari, Z. Jiang, T. S. Reynolds, N. E. Bernskoetter, A. F. Szczodroski, K. J. Bassuner, D. L. Kirkpatrick, T. L. Rold, G. L. Sieckman, T. J. Hoffman, J. P. Connors, C. J. Smith, Synthesis and biological evaluation of copper-64 radiolabeled [DUPA-6-Ahx-(NODAGA)-5-Ava-BBN(7-14)NH2], a novel bivalent targeting vector having affinity for two distinct biomarkers (GRPr/PSMA) of prostate cancer, Nuclear Medicine and Biology 41 (4) (2014) 355–363. arXiv:NIHMS150003, doi:10.1016/j.nucmedbio.2014.01.001.

[8] E. Gourni, L. Del Pozzo, E. Kheirallah, C. Smerling, B. Waser, J.-C. Reubi, B. M. Paterson, P. S. Donnelly, P. T. Meyer, H. R. Maecke, Copper-64 Labeled Macrobicyclic Sarcophagine Coupled to a GRP Receptor Antagonist Shows Great Promise for PET Imaging of Prostate Cancer, Molecular Pharmaceutics 12 (8) (2015) 2781–2790. doi:10.1021/mp500671j.

[9] T. W. Burrows, Nuclear Data Sheets for A = 47, Nuclear Data Sheets 108 (5) (2007) 923–1056. doi:10.1016/j.nds.2007.04.002.

[10] S. M. Qaim, R. Capote, F. Tarkanyi, Nuclear Data for the Production of Therapeutic Radionuclides, Tech. Rep. 473 (2011).

[11] S. M. Qaim, Nuclear data for production and medical application of radionuclides: Present status and future needs, Nuclear Medicine and Biology 44 (2016) 31–49. doi:10.1016/j.nucmedbio.2016.08.016.

[12] K. L. Kolsky, V. Joshi, L. F. Mausner, S. C. Srivastava, Radiochemical purification of no-carrier-added scandium-47 for radioimmunotherapy, Applied Radiation and Isotopes 49 (12) (1998) 1541–1549. doi:10.1016/S0969-8043(98)00016-5.

[13] L. F. Mausner, V. Joshi, K. L. Kolsky, Evaluation of chelating agents for radioimmunotherapy with scandium-47, Journal of Nuclear Medicine 36 (CONF-950603–).

[14] E. Browne, J. K. Tuli, Nuclear Data Sheets for A = 99, Nuclear Data Sheets 112 (2) (2011) 275–446. doi:10.1016/j.nds.2011.01.001.

[15] C. Müller, M. Bunka, S. Haller, U. Köster, V. Groehn, P. Bernhardt, N. van der Meulen, A. Türler, R. Schibli, Promising Prospects for 44Sc-/47Sc-Based Theragnostics: Application of 47Sc for Radionuclide Tumor Therapy in Mice, Journal of Nuclear Medicine 55 (10) (2014) 1658–1664. doi:10.2967/jnumed.114.141614.

[16] L. Deilami-nezhad, L. Moghaddam-Banaem, M. Sadeghi, M. Asgari, Production and purification of Scandium-47: A potential radioisotope for cancer theranostics, Applied Radiation and Isotopes 118 (2016) 124–130. doi:10.1016/j.apradiso.2016.09.004.

[17] K. S. Bhatki, A. T. Rane, M. B. Kabadi, Preparation of carrier-free copper-64, 67 nuclides by liquid-liquid extraction, Journal of Radioanalytical Chemistry 2 (1-2) (1969) 73–77.

[18] S. Mirzadeh, F. F. Knapp, Spontaneous electrochemical separation of carrier-free copper-64 and copper-67 from zinc targets, Radiochimica Acta 57 (4) (1992) 193–200.

[19] H. F. Aly, M. A. El-Haggan, Production of carrier-free scandium radioisotopes from a neutron-irradiated potassium titanium oxalate target, Microchimica Acta 59 (1) (1971) 4–8. doi:10.1007/BF01216875.

[20] T. H. Bokhari, A. Mushtaq, I. U. Khan, Separation of no-carrier-added radioactive scandium from neutron irradiated titanium, Journal of Radioanalytical and Nuclear Chemistry 283 (2) (2010) 389–393. doi:10.1007/s10967-009-0370-6.

[21] L. Pietrelli, L. Mausner, K. Kolsky, Separation of carrier-free 47Sc from titanium targets, Journal of Radioanalytical and Nuclear Chemistry 157 (2) (1992) 335–345. doi:10.1007/BF02047448.

[22] H. Liskien, A. Paulsen, Neutron production cross sections and energies for the reactions T(p,n)3He, D(d,n)3He, and T(d,n)4He, Atomic Data and Nuclear Data Tables 11 (7) (1973) 569–619. doi:10.1016/S0092-640X(73)80081-6.

[23] R. Capote, K. I. Zolotarev, V. G. Pronyaev, A. Trkov, Updating and Extending the IRDF-2002 Dosimetry Library, Journal of ASTM International 9 (4) (2012) 1–9. doi:10.1520/JAI104119.

[24] E. M. Zsolnay, R. Capote, H. J. Nolthenius, A. Trkov, Summary Description of the New International Reactor Dosimetry and Fusion File (IRDFF release 1.0), IAEA Technical Report INDC (NDS)-0616.

[25] J. T. Goorley, M. R. James, T. E. Booth, F. B. Brown, J. S. Bull, L. J. Cox, J. W. J. Durkee, J. S. Elson, M. L. Fensin, R. A. I. Forster, J. S. Hendricks, H. G. I. Hughes, R. C. Johns, B. C. Kiedrowski, R. L. Martz, S. G. Mashnik, G. W. McKinney, D. B. Pelowitz, R. E. Prael, J. E. Sweezy, L. S. Waters, T. Wilcox, A. J. Zukaitis, Initial MCNP6 release Overview - MCNP6 version 1.0, LA-UR-13-22934.

[26] J. Blachot, Nuclear Data Sheets for A = 113, Nuclear Data Sheets 111 (6) (2010) 1471–1618. doi:10.1016/j.nds.2010.05.001.

[27] J. Blachot, Nuclear Data Sheets for A = 115, Nuclear Data Sheets 113 (10) (2012) 2391–2535. doi:10.1016/j.nds.2012.10.002.

[28] J. Blachot, Nuclear Data Sheets for A = 116, Nuclear Data Sheets 111 (3) (2010) 717–895. doi:10.1016/j.nds.2010.03.002.

[29] D. C. Radford, Notes on the use of the program gf3 (2000).

[30] D. C. Radford, ESCL8R and LEVIT8R: Software for interactive graphical analysis of HPGe coincidence data sets, Nuclear Inst. and Methods in Physics Research, A 361 (1-2) (1995) 297–305. doi:10.1016/0168-9002(95)00183-2.

[31] C. D. Nesaraja, S. D. Geraedts, B. Singh, Nuclear Data Sheets for A = 58, Nuclear Data Sheets 111 (4) (2010) 897–1092. doi:10.1016/j.nds.2010.03.003.

[32] N. Otuka, E. Dupont, V. Semkova, B. Pritychenko, A. I. Blokhin, M. Aikawa, S. Babykina, M. Bossant, G. Chen, S. Dunaeva, R. A. Forrest, T. Fukahori, N. Furutachi, S. Ganesan, Z. Ge, O. O. Gritzay, M. Herman, S. Hlavač, K. Kato, B. Lalremruata, Y. O. Lee, A. Makinaga, K. Matsumoto, M. Mikhaylyukova, G. Pikulina, V. G. Pronyaev, A. Saxena, O. Schwerer, S. P. Simakov, N. Soppera, R. Suzuki, S. Takács, X. Tao, S. Taova, F. Tárkányi, V. V. Varlamov, J. Wang, S. C. Yang, V. Zerkin, Y. Zhuang, Towards a More Complete and Accurate Experimental Nuclear Reaction Data Library (EXFOR): International Collaboration Between Nuclear Reaction Data Centres (NRDC), Nuclear Data Sheets 120 (2014) 272–276. doi:10.1016/j.nds.2014.07.065.

[33] J. Rapaport, J. J. van Loef, Excitation Function of the Reaction Zn-64(n, p)Cu-64 with Neutrons of Energies between 2 and 3.6 Mev, Phys. Rev. 114 (2) (1959) 565–569. doi:10.1103/PhysRev.114.565.

[34] K. Nakai, H. Gotoh, H. Amano, Excitation Functions of Ni58(n, p)Co58 and Zn64(n, p)Cu64 Reactions in the Energy Region from 1.8 to 4.8 Mev, Journal of the Physical Society of Japan 17 (8) (1962) 1215–1223. doi:10.1143/JPSJ.17.1215.

[35] A. Paulsen, H. Liskien, Cross-sections for some (n, p) reactions near threshold, in: Nuclear data for reactors. Proceedings of a conference on nuclear data-microscopic cross-sections and other data basic for reactors., Paris, 1967, pp. 217–224.

[36] D. C. Santry, J. P. Butler, Excitation Curves for the Reactions of Fast Neutrons with Zinc, Canadian Journal of Physics 50 (20) (1972) 2536–2548. doi:10.1139/p72-336.

[37] D. L. Smith, J. W. Meadows, Cross-Section Measurement of (n, p) Reactions for 27Al, 46,47,48Ti, 58Ni, 59Co, and 64Zn from Near Threshold to 10 MeV, Nuclear Science and Engineering 58 (3) (1975) 314–320.

[38] C. King, C. Ai, J. Chou, Cross-section measurement for the reaction Zn-64(n,p) Cu-64, Nuclear Science, Taiwan 16 (6) (1979) 71.

[39] H. Hussain, S. Hunt, Absolute neutron cross section measurements in the energy range between 2 and 5 MeV, The International Journal of Applied Radiation and Isotopes 34 (4) (1983) 731–738. doi:10.1016/0020-708X(83)90252-1.

[40] Y. Ikeda, C. Konno, M. Mizumoto, K. Hasegawa, S. Chiba, Y. Yamanouchi, M. Sugimoto, Activation cross section measurement at neutron energies of 9.5, 11.0, 12.0 and 13.2 MeV using H-1(B-11,n)C-12 neutron source at JAERI, in: S. M. Qaim (Ed.), Proceedings of an International Conference, held at the Forschungszentrum Jülich, Fed. Rep. of Germany, 13-17 May 1991, Springer-Verlag Berlin Heidelberg, Juelich, Germany, 1990, pp. 294–296.

[41] T. Shimizu, H. Sakane, S. Furuichi, M. Shibata, K. Kawade, H. Takeuchi, An improved pneumatic sample transport system for measurement of activation cross-sections with d-D neutrons in the energy range between 2.1 and 3.1 MeV, Nuclear Instruments and Methods in Physics Research Section A: Accelerators, Spectrometers, Detectors and Associated Equipment 527 (3) (2004) 543–553. doi:10.1016/j.nima.2004.03.184.

[42] L. González, A. Trier, J. J. van Loef, Excitation Function of the Reaction Ti-47(n, p)Sc-47 at Neutron Energies between 2.0 and 3.6 Mev, Phys. Rev. 126 (1) (1962) 271–273. doi:10.1103/PhysRev.126.271.

[43] F. Armitage, 47Ti(n,p) Cross-section from 2.19 To 3.64 MeV, Priv.Comm: J. Symonds (1967).

[44] Y. Ikeda, C. Konno, K. Kosako, K. Oishi, Activation Cross Section Measurement at a Neutron Energy Range from 2.1 to

3.0 Mev by D-D Neutron Source at FNS, Japanese Report to NEANDC 155 (1990) 11.

[45] T. Senga, H. Sakane, M. Shibata, H. Yamamoto, K. Kawade, Y. Kasugai, Y. Ikeda, H. Takeuchi, T. Furuta, Measurement of neutron activation cross sections in the energy range between 2. and 7. MeV by using a Ti-deuteron Target and a deuteron gas target, in: Proceedings of the JAERI Conference 2000, Japan, 2000, p. 5.

[46] T. Shimizu, H. Sakane, M. Shibata, K. Kawade, T. Nishitani, Measurements of activation cross sections of (n, p) and (n, α) reactions with d-D neutrons in the energy range of 2.1-3.1 MeV, Annals of Nuclear Energy 31 (9) (2004) 975–990. doi:10.1016/j.anucene.2003.12.005.

[47] M. B. Chadwick, M. Herman, P. Oblozinsky, M. E. Dunn, Y. Danon, A. C. Kahler, D. L. Smith, B. Pritychenko, G. Arbanas, R. Arcilla, R. Brewer, D. A. Brown, R. Capote, A. D. Carlson, Y. S. Cho, H. Derrien, K. Guber, G. M. Hale, S. Hoblit, S. Holloway, T. D. Johnson, T. Kawano, B. C. Kiedrowski, H. Kim, S. Kunieda, N. M. Larson, L. Leal, J. P. Lestone, R. C. Little, E. A. McCutchan, R. E. MacFarlane, M. MacInnes, C. M. Mattoon, R. D. McKnight, S. F. Mughabghab, G. P. A. Nobre, G. Palmiotti, A. Palumbo, M. T. Pigni, V. G. Pronyaev, R. O. Sayer, A. A. Sonzogni, N. C. Summers, P. Talou, I. J. Thompson, A. Trkov, R. L. Vogt, S. C. van der Marck, A. Wallner, M. C. White, D. Wiarda, P. G. Young, ENDF/B-VII.1 nuclear data for science and technology: Cross sections, covariances, fission product yields and decay data, Nuclear Data Sheets 112 (12) (2011) 2887–2996. doi:10.1016/j.nds.2011.11.002.

[48] A. J. Koning, D. Rochman, Modern Nuclear Data Evaluation with the TALYS Code System, Nuclear Data Sheets 113 (12) (2012) 2927–2934. doi:10.1016/j.nds.2012.11.002.

[49] S.-C. Wu, Nuclear Data Sheets for A = 46, Nuclear Data Sheets 91 (1) (2000) 1–116. doi:10.1006/ndsh.2000.0014.